Biochemical and Biophysical Research Communications 450 (2014) 1045–1050

Contents lists available at ScienceDirect

Biochemical and Biophysical Research Communications

journal homepage: www.elsevier.com/locate/ybbrc

ATP-binding mode including a carbamoylated lysine and two Mg^{2+} ions, and substrate-binding mode in *Acinetobacter baumannii* MurF

Sun-Shin Cha [a,b,c,*,1], Young Jun An [a,1], Chang-Sook Jeong [a], Jeong Hee Yu [d], Kyung Min Chung [d,e,*]

[a] Marine Biotechnology Research Division, Korea Institute of Ocean Science and Technology, Ansan 426-744, Republic of Korea
[b] Department of Convergence Study on the Ocean Science and Technology, Ocean Science and Technology School, Pusan 606-791, Republic of Korea
[c] Department of Marine Biotechnology, Korea University of Science and Technology, Daejeon 305-333, Republic of Korea
[d] Department of Microbiology and Immunology, Chonbuk National University Medical School, Jeonju 561-756, Republic of Korea
[e] Institute for Medical Science, Chonbuk National University Medical School, Jeonju 561-756, Republic of Korea

ARTICLE INFO

Article history:
Received 18 June 2014
Available online 27 June 2014

Keywords:
Crystal structure
MurF–ATP complex
MurF–ATP–UDP complex
Carbamoylated lysine
Magnesium

ABSTRACT

MurF adds D-Ala-D-Ala dipeptide to UDP-*N*-acetylmuramyl-L-Ala-γ-D-Glu-*m*-DAP (or L-Lys) in an ATP-dependent manner, which is the last step in the biosynthesis of monomeric precursor of peptidoglycan. Here we report crystal structures of two MurF–ATP complexes: the MurF–ATP complex and the MurF–ATP–UDP complex. The ATP-binding mode revealed by the crystal structure of the MurF–ATP complex confirms the previous biochemical demonstration that a carbamoylated lysine and two Mg^{2+} ions are required for enzyme activity of MurF. The UDP–MurF interactions observed in the crystal structure of the MurF–ATP–UDP complex depict the characteristic substrate-binding mode of MurF. The emergence and dissemination of multidrug-resistant *Acinetobacter baumannii* strains are great threats to public health. Therefore, the structural information on *A. baumannii* MurF as a validated target for drug discovery will provide a framework to develop antibacterial agents against multidrug-resistant *A. baumannii* infections as well as to understand the reaction mechanism of MurF.

1. Introduction

Acinetobacter baumannii, a gram-negative pathogen, causes serious nosocomial infections that are associated with high mortality, prolonged hospital stay, and increased medical costs [1–3]. Although the pathogen was recognized as a serious opportunistic pathogen of hospital acquired infection in the intensive care unit, the infection has also occurred in the community, in the long-term care facilities, and in wounded military personnel in the last decade [1–3]. The use of broad-spectrum antibiotics and the remarkable ability of *A. baumannii* to acquire antibiotic resistance cause a great threat to public health [4,5]. Thus, given the rapid emergence of multidrug-resistance and refractoriness of existing antimicrobial agents, novel approaches and discovery of targets are required to prevent and treat *A. baumannii* infections.

Many clinically-used antibiotics have been successfully developed against enzymes for peptidoglycan synthesis [6]. The peptidoglycan is a mesh-like rigid layer composed of cross-linked glycan chains. *N*-acetylglucosamine (GlcNAc) and *N*-acetylmuramic acid (MurNAc) linked by β-1,4-glycosidic bonds are the repeating units to form linear glycan chains. Short peptides consisting of L-alanine, D-alanine, D-glutamic acid, and either L-lysine or *meso*-diaminopimelic acid (*m*-DAP) that are attached to each MurNAc residue in glycan chains are exploited to cross-link glycan chains. UDP-GlcNAc and UDP-MurNAc are nucleotide precursors of GlcNAc and MurNAc, respectively. UDP-GlcNAc is synthesized from fructose-6-phosphate and UDP-MurNAc is formed from UDP-GlcNAc. The attachment of amino acids to the UDP-MurNAc moiety is catalyzed by four ATP-dependent ligases which sequentially add L-alanine (MurC), D-glutamic acid (MurD), *meso*-diaminopimelic acid or L-lysine (MurD), and D-alanine-D-alanine (MurF) to the D-lactoyl group of UDP-MurNAc [7].

Given that MurF is involved in peptidoglycan biosynthesis and there is no counterpart in human hosts, MurF is an attractive target to develop antibiotics. In fact, several inhibitors have been developed against the MurF proteins from some pathogenic bacteria including *Streptococcus pneumonia*, *Staphylococcus aureus*, and *Escherichia coli* [8,9]. Here, we report the crystal structures of the

* Corresponding authors. Address: Marine Biotechnology Research Division, Korea Institute of Ocean Science and Technology, Ansan 426-744, Republic of Korea (S.-S. Cha). Address: Department of Microbiology and Immunology, Chonbuk National University Medical School, Jeonju 561-756, Republic of Korea (K.M. Chung).
E-mail addresses: chajung@kiost.ac (S.-S. Cha), kmin@jbnu.ac.kr (K.M. Chung).
[1] These authors equally contributed to this work.

http://dx.doi.org/10.1016/j.bbrc.2014.06.108
0006-291X/

A. baumannii MurF (*Ab*MurF)–ATP complex and the *Ab*MurF–ATP–UDP complex. Although crystal structures of *E. coli* MurF, *Thermotoga maritima* MurF, and *S. pneumonia* MurF whose sequence identities to *Ab*MurF are 41%, 32%, and 29%, respectively, are available [8–11], so far there is no structural information on the ATP complexes of MurF. Therefore the structural information on the two ATP complexes will provide an important framework for deciphering the enzyme mechanism of *Ab*MurF and for the structure-based development of inhibitors to treat *A. baumannii* infections.

2. Materials and methods

2.1. Crystallization, phasing, model building, and refinement

We have previously reported expression, purification, and crystallization of selenomethionine substituted *Ab*MurF (Se-*Ab*MurF) [13]. Trigonal crystals of Se-*Ab*MurF with ATP were grown in a precipitant solution containing 20% (*w/v*) polyethylene glycol (PEG) 3000 and 0.1 M sodium citrate: citric acid pH 5.5. Crystals belonged to space group $P322_1$, with unit-cell parameters $a = b = 85.42$, $c = 129.86$ Å corresponding to one complex per asymmetric unit. A 1.9 Å resolution MAD data set was collected on beamline 5C of Pohang Light Source (Pohang, Republic of Korea) (Table S1). Fourteen selenium positions of Se-*Ab*MurF were located and phases were calculated using the AutoSol program [13] in PHENIX [14], giving rise to an auto-built model with R_{work}/R_{free} of 23.71/27.05. Without further refinement, this auto-built model was used as a search model to determine the structures of the *Ab*MurF–ATP–UDP complex and the *Ab*MurF–ATP complex by molecular replacement.

Crystals of the *Ab*MurF–ATP–UDP complex were obtained by soaking experiments. Trigonal crystals of the *Ab*MurF–ATP complex isomorphous to those of the Se-*Ab*MurF–ATP complex were grown in the mother liquor described above and then crystals were transferred to a solution containing 20% glycerol, 20% PEG 3000, 0.1 M sodium citrate: citric acid pH 5.5, and 15 mM UDP. After 25 min soaking, a crystal was mounted and 1.8 Å resolution diffraction data was collected on beamline 5C of Pohang Light Source (Table 1).

Monoclinic crystals of the *Ab*MurF–ATP complex were grown in a precipitant solution containing 24% PEG 4000, 0.08 M Tris–HCl pH 8.5, 0.16 M magnesium chloride, and 20% glycerol by the micro-batch crystallization method at 295 K. A 2.8 Å data set was collected on beamline 5C of Pohang Light Source (Pohang, Republic of Korea) (Table 1). Crystals belonged to space group $P2_1$ with cell parameters $a = 44.56$, $b = 89.72$, $c = 126.90$ Å and $\beta = 93.45$ corresponding to two complexes per asymmetric unit.

Diffraction data were processed with HKL-2000 [15]. Molrep [16] was used for molecular replacement. Residues were traced in the electron density and modeled with COOT [17]. Refinement was carried out with CNS [18] (the *Ab*MurF–ATP–UDP complex) or PHENIX [14] (the *Ab*MurF–ATP complex) (Table 1). The Ramachandran plots of the final models indicate that 96.4% (the *Ab*MurF–ATP complex) and, 94.7% (the *Ab*MurF–ATP–UDP complex) of the non-glycine residues are in the most favored regions and that the remaining 3.1% (the *Ab*MurF–ATP complex) and, 4.2% (the *Ab*MurF–ATP–UDP complex) residues are in allowed regions.

2.2. PDB accession numbers

The atomic coordinates and structure factors of the *Ab*MurF–ATP complex and the *Ab*MurF–ATP–UDP complex have been deposited in the Protein Data Bank, with the accession code 4QF5 and 4QDI, respectively.

Table 1
Data collection and refinement.

	*Ab*MurF–ATP	*Ab*MurF–ATP–UDP
Data collection		
Wavelength (Å)	1.00000	1.00000
Resolution range (Å)	50–2.80	50–1.80
Total no. of reflections	456,549	885,596
No. of unique reflections	24,942 (1208)	50,545 (2500)
Completeness (%)[a]	99.7 (99.6)	97.3 (96.2)
Redundancy	4.3 (4.5)	8.4 (6.3)
I/σ (I)[a]	25.5 (5.4)	41.9 (3.8)
R_{sym} (%)[a,b]	13.0 (62.6)	5.7 (33.9)
Refinement statistics		
Resolution range (Å)	37.44–2.8	37.48–1.8
No. reflections	24,046	50,542
No. atoms		
Protein	6913	3444
Magnesium	4	1
ATP	62	31
UDP		24
Ethylene glycol		8
Water		265
B-factors		
Protein	32.11	37.54
Magnesium	30.69	51.83
ATP	25.31	36.36
UDP		51.33
Ethylene glycol		34.15
Water		38.03
R^c (R_{free}) (%)	19.19 (24.90)	22.70 (25.30)
r.m.s. Deviations[d]		
Bonds length (Å)	0.010	0.005
Bond angles (°)	1.246	1.2

[a] The number in parentheses is for the outer shell.
[b] $R_{sym} = \sum_h \sum_l |I_{h,i} - I_h| / \sum_h \sum_l \sum \sum I_{h,i}$, where I_h is the mean intensity of the i observations of symmetry related reflections of h.
[c] $R = \sum |F_o - F_c| / \sum F_o$, where $F_o = F_p$, and F_c is the calculated protein structure factor from the atomic model. R_{free} was calculated with 10% of the reflections.
[d] r.m.s. Deviations in bond length and angles are the deviations from ideal values.

3. Results

3.1. Overall structure of AbMurF

The final model for the *Ab*MurF–ATP–UDP complex contains residues 9-465, one ATP molecule, one UDP molecule, one Mg^{2+} ion, two ethylene glycol molecules, and 265 water molecules. The final models for two *Ab*MurF–ATP complexes in the asymmetric unit of monoclinic crystals contain residues 7-465, one ATP molecule, two Mg^{2+} ions of one copy (molecule A) and residues 9-465, one ATP molecule, and two Mg^{2+} ions for the other copy (molecule B). Molecules A and B are superposed with rmsd 0.49 for all the equivalent Cα atoms. Hereafter we describe only molecule A. *Ab*MurF is composed of three contiguous domains: the N-terminal, the central, and the C-terminal domains (Fig. 1 and Fig. S1). The N-terminal domain (residues 7-95) has a five-stranded β-sheet (β1, β2, β3, β4 and β5). The solvent-exposed face of the sheet is packed with a stretched loop between β3 and β4, a helix (α2), and a 3_{10} helix (η2) whereas the other face of the sheet with one helix (α1) and one 3_{10} helix (η1) mediates domain-domain contact with the adjacent central domain. The central domain (residues 96-319) assumes a four-layered structure composed of a helical region containing seven helices (α3, α5, α6, α7, α8, α9, and η3), a six-stranded parallel sheet (β6, β7, β8, β9, β10, and β11), a three-helix bundle (α4, α10 and α11), and a three-stranded sheet (β12, β13, and β14). The C-terminal domain (residues 329-465) has a six-stranded sheet (β15, β16, β17, β18, β19, and β20) sandwiched by seven helices (α12, α13, α14, α15, α16, η4, and η5). There is a hinge loop (residues 320-328) between the central and the C-terminal domains.

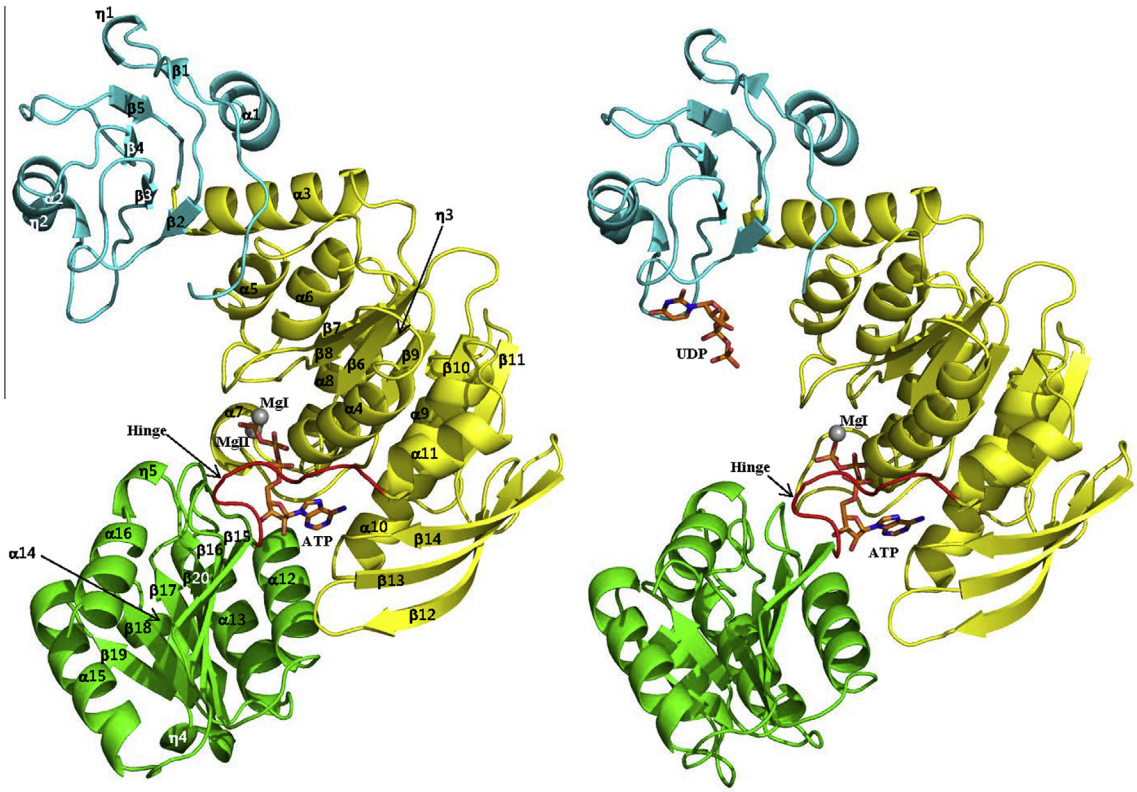

Fig. 1. Ribbon diagrams of the *Ab*MurF–ATP complex (left) and the *Ab*MurF–ATP–UDP complex (right) shown with secondary structures labeled. The N-terminal, the central, and the C-terminal domains are colored in cyan, yellow, and green, respectively. ATP and UDP are shown in sticks. Magnesium ions are represented in gray spheres. The hinge loop between the central and the C-terminal domains is colored in red. (For interpretation of the references to color in this figure legend, the reader is referred to the web version of this article.)

3.2. ATP-binding mode

ATP is situated at the interface between the central and the C-terminal domains (Fig. 1) and makes multiple interactions with residues of MurF (Fig. 2A). The adenine base fits into a space surrounded by Ser123, His292, and Asn296 in the central domain, and Ser349 and Ala352 in the C-terminal domain. N1 and NH2 at C-6 form polar interactions with the side chain amide of Asn296. The interaction of Asn296 with NH2 at C-6 that does not exist in other bases is probably responsible for the ATP specificity of MurF [19]. The ribose 3′–OH is in hydrogen bond distances from the side-chain carboxyl group of Asp341 and the amine group of Lys448 in the C-terminal domain. The α- and β-phosphates make multiple hydrogen bonds with the backbone nitrogen atoms of the N-terminal end of α4 (residues 124-127) in the central domain. In addition, the triphosphate moiety makes multiple charged or polar interactions with the side chains of Lys125, Asn150, and Arg327 in the central domain. Remarkably, there are two Mg^{2+} ions: the first one (MgI) is coordinated by β, γ-phosphates of ATP and two residues (Thr126 and Glu172) in the central domain and the second one (MgII) is surrounded by γ-phosphate, His202, and a carbamoylated Lys216. The strong difference Fourier electron density map around the side-chain amino group of Lys216 indicates that this residue is chemically modified. Since a carbamoylated lysine was suggested to be essential for metal binding in MurF [20] and a carbamoylated lysine was nicely fitted into the electron density, we concluded the carbamylation of Lys216.

3.3. UDP-binding mode

UDP binds to the border between the N-terminal and the central domains with an excellent electrostatic complementarity (Figs. 1 and 2B). The uracil ring makes π–π stacking interaction with the benzyl side chain of Phe61 in the N-terminal domain. The ribose ring sits on the hydrophobic region at the domain interface with its 2′–OH engaged in hydrogen bonding with the hydroxyl group of Thr42. α-Phosphate forms electrostatic interactions with the side-chain guanidinium group of Arg97 in the central domain.

3.4. Structural disparity between the AbMurF–ATP complex and the AbMurF–ATP–UDP complex

MgII and the carbamylated Lys216 that is essential for MgII-binding exist only in the *Ab*MurF–ATP complex whereas they are absent from the *Ab*MurF–ATP–UDP complex. The presence of MgII induces three conformational changes in the *Ab*MurF–ATP complex compared to the *Ab*MurF–ATP–UDP complex: the helical transformation of the β9–α7 loop (the connecting loop between β9 and α7), the further rotation of the C-terminal domain toward the central domain, and the displacement of the β8–α6 loop (Fig. 3). The β9–α7 loop contains His202, a ligand of MgII. The β9–α7 loop adopts a helical conformation to locate His202 in the coordination shell of MgII in the *Ab*MurF–ATP complex whereas the loop with an extended conformation stays away from the MgII site in the *Ab*MurF–ATP–UDP complex. The transition of the β9–α7 loop into the helical conformation is accompanied by the rotation of the C-terminal domain and a conformational change of the β8–α6 loop. The helical conformational change generates ~5 Å space between the central and the C-terminal domains. As a result, the C-terminal domain rotates more towards the central domain in the *Ab*MurF–ATP complex than in the *Ab*MurF–ATP–UDP complex. In the *Ab*MurF–ATP complex, Phe206 of the helical β9–α7 loop extends

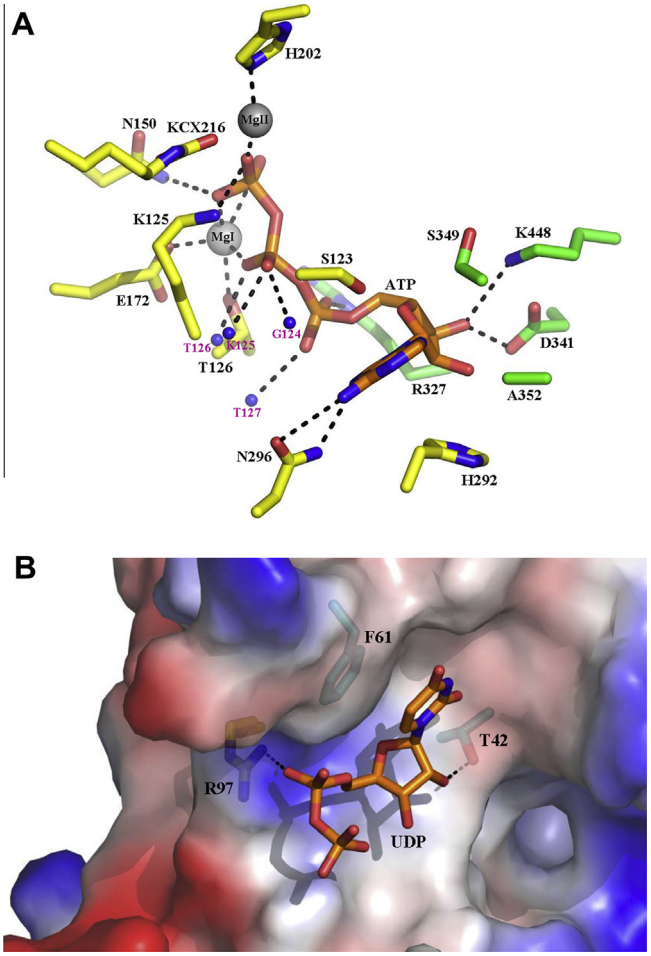

Fig. 2. ATP-binding mode and UDP-binding mode. ATP and UDP are shown in orange sticks. Residues from the N-terminal, the central, and the C-terminal domains are shown in sticks and are colored in cyan, yellow, and green, respectively. Magnesium ions are represented in gray spheres. Small spheres in blue represent backbone nitrogen atoms. Water molecules are in red spheres. Black dotted lines point out interatomic interactions, and oxygen and nitrogen atoms are colored in red and blue, respectively. (A) Interactions between ATP and *Ab*MurF in the *Ab*MurF–ATP complex. KCX216 indicates the carbamoylated Lys216. (B) Interactions between UDP and *Ab*MurF in the *Ab*MurF–ATP–UDP complex. *Ab*MurF is represented as a transparent surface with electrostatic potentials shown. Positive, neutral, and negative electrostatic potentials are colored blue, white, and red, respectively. (For interpretation of the references to color in this figure legend, the reader is referred to the web version of this article.)

towards the β8–α6 loop and thus the β8–α6 loop moves back from Phe206 to avoid steric clash with the bulky benzyl group.

Due to the absence of MgII and the carbamoylated lysine, and the consequent arrangement of the C-terminal domain, the ATP-binding mode in the *Ab*MurF–ATP–UDP complex is incomplete compared to that in the *Ab*MurF–ATP complex (Fig. S2). Although MgI is coordinated in the same way, interactions between ATP and *Ab*MurF are changed. The adenine base interacts only with residues of the central domain without contact with the C-terminal domain. The 2′–OH and 3′–OH of ribose make two water-mediated interactions with Asp341 in the C-terminal domain. The α- and β-phosphates make multiple hydrogen bonds with the backbone nitrogen atoms of residues (residues 124-127) of the central domain. In addition, Lys125 in the central domain makes salt bridges with β- and γ-phosphates and the guanidinium side chain of Arg327 in the C-terminal domain makes a salt bridge with α-phosphate. γ-Phosphate makes a polar contact with Tyr343 in the C-terminal domain.

4. Discussion

4.1. Conformational plasticity of the C-terminal domain in MurF

The crystal structures depicting three different states of MurF have been reported. The crystal structure of the *E. coli* MurF apo-enzyme revealed that the three domains are linearly arranged to assume a crescent-like conformation (Fig. 4) [10]. In contrast to the open conformation in which domain–domain contacts occur only between adjacent domains, the three domains are rolled up to form a closed conformation in which the C-terminal domain contacts with both the N-terminal and the central domains in the crystal structures of *S. pneumonia* MurF in complex with inhibitors (Fig. 4) [8,9]. In this conformation, the ATP-binding site is collapsed, indicating that this closed conformation is not an active conformation. In the case of the ADP-bound structure of *T. maritima* MurF [11], it adopts a conformation that is between the open and closed states (Fig. 4). Structural superposition of all the MurF structures including *Ab*MurF structures presented here shows that the variation in the relative position of the C-terminal domain is responsible for the observed conformational disparity among the MurF structures, indicating that MurF has a hinge between the central and the C-terminal domains (Figs. 1 and 4). In contrast to the extensive contact between the N-terminal and the central domains, there are few direct interactions between the central and the C-terminal domains that are simply linked by a connecting loop in the apo MurF structure. The flexible connection loop and few interdomain interactions between the central and the C-terminal domains support the innate flexibility at the hinge.

According to kinetic studies, ATP-binding is the first event in the MurF-catalyzed reaction that is followed by the sequential binding of UDP-*N*-acetylmuramyl-tripeptide and D-Ala-D-Ala [21]. ATP-binding to the interface between the central and the C-terminal domains induces the conformational change from a crescent-like conformation to an ATP-bound conformation (Fig. 4), suggesting that the ATP-bound conformation is a prerequisite for substrate binding to MurF. Consequently, the conformational freedom of the C-terminal domain that allows MurF to adopt the ATP-bound conformation plays critical roles in the enzyme reaction.

4.2. Insights into the enzymatic mechanism of MurF

MurC, MurD, MurE, and MurF catalyze the assembly of the peptide moiety by successive additions of L-Ala (MurC), D-Glu (MurD), *m*-DAP or L-Lys (MurE), and D-Ala-D-Ala (MurF) to UDP-MurNAc through the same reaction mechanism. The γ-phosphate of ATP is transferred to the C-terminal carboxylate of UDP-precursors to form an acyl phosphate intermediate, the carbonyl carbon of which is subsequently attacked by the amino group of the incoming amino acid to form a peptide bond releasing the phosphate group [22,23]. MurD is the best-characterized enzyme among the Mur ligases. Structural information on MurD in complex with UDP-precursor, ADP, and/or Mg^{2+} revealed the involvement of two Mg^{2+} ions and one carbamoylated lysine in its catalytic activity [20]. The functional requirement of two Mg^{2+} ions and a carbamoylated lysine in the catalytic activity of MurF has also been biochemically established [24], which has not been structurally demonstrated so far. The crystal structure of the *Ab*MurF–ATP complex depicting the ATP-binding mode involving two Mg^{2+} ions and a carbamoylated lysine (Lys216) ascertains the previous biochemical establishment. The carbamoylated lysine has previously been proposed to be essential for Mg^{2+} binding [20]. Consistently, the carbamoylated lysine is located in the vicinity of MgII although the distance between the carbamoylated lysine and MgII (~3.3 Å) excludes the direct coordination of MgII. It is worth of note that the carba-

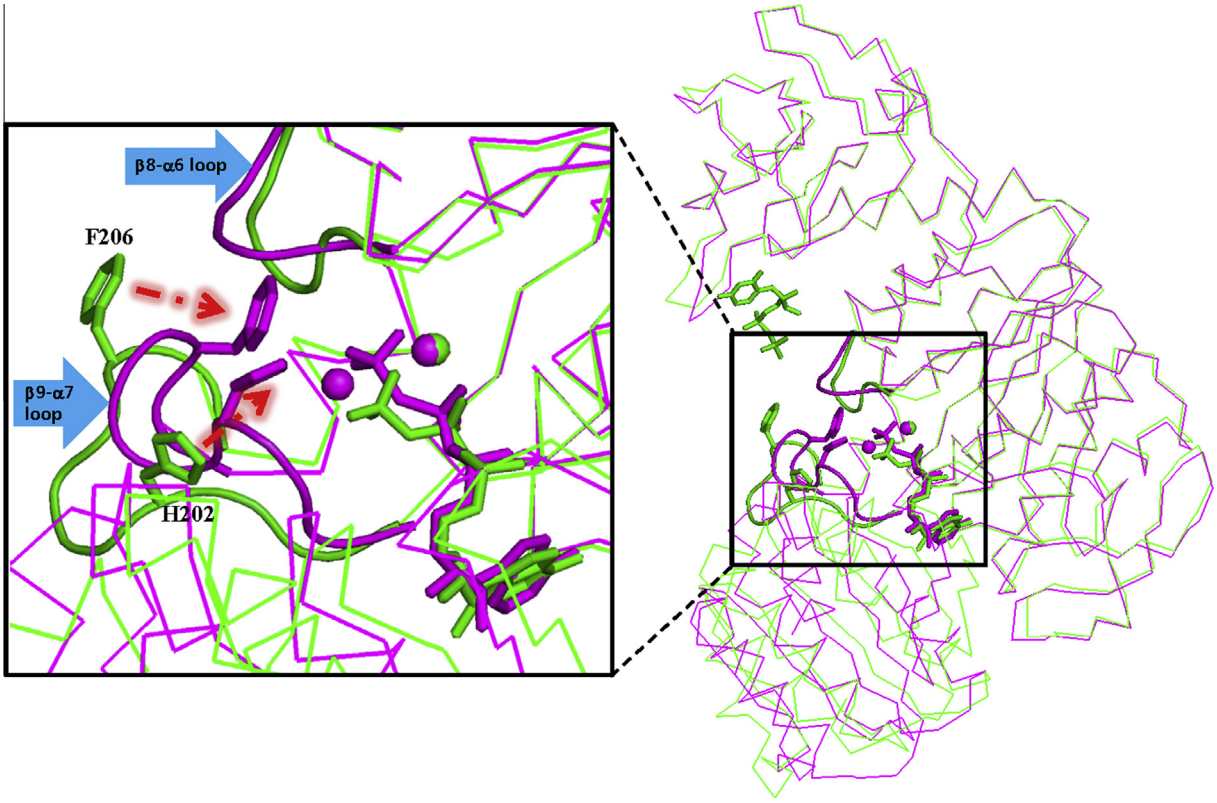

Fig. 3. Superposed Cα tracing of the *Ab*MurF–ATP complex (magenta) and the *Ab*MurF–ATP–UDP complex (green). ATP/UDP and magnesium ions are represented by sticks and spheres, respectively. Phe206 and His202 are in sticks. For clarity, the β8–α6 loop and the β9–α7 loop are thickly shown. (For interpretation of the references to color in this figure legend, the reader is referred to the web version of this article.)

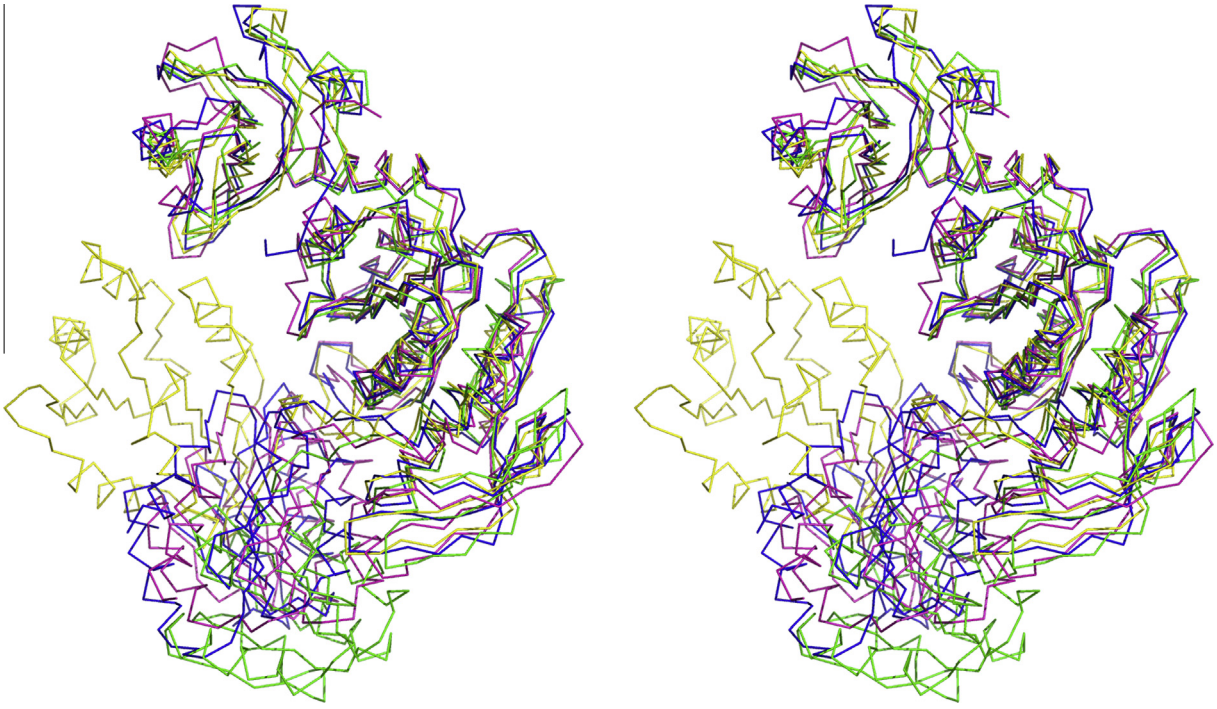

Fig. 4. Superposed Cα tracing of all the available MurF structures; *Ab*MurF (blue), *E. coli* MurF (green) *S. pneumonia* MurF (yellow), and *T. maritima* MurF (magenta). (For interpretation of the references to color in this figure legend, the reader is referred to the web version of this article.)

moylated lysine takes part in Mg^{2+} coordination through water molecules in MurD [20]. It should be noted that water molecules that coordinate MgII cannot be seen in the 2.8 Å resolution crystal structure of the *Ab*MurF–ATP complex.

The functional role of MgII seems to be the proper and proximal positioning of reacting groups in the active site, which significantly contributes to the catalytic power of MurF. The position of γ-phosphate in ATP is different between the *Ab*MurF–ATP–UDP complex

without MgII and the *Ab*MurF–ATP complex with MgII (Fig. 3). The γ-phosphate in the *Ab*MurF–ATP complex extends towards the central domain to coordinate MgII, which generates a hydrogen bond with Asn150 (Fig. 2A). According to the crystal structure of the MurD–ADP–Mg^{2+}–UMA (UDP-*N*-acetylmuramyl-L-alanine) complex, the carboxylate of UMA that attacks the phosphorus of γ-phosphate takes part in MgII coordination [20]. When UDP-*N*-acetylmuramyl-tripeptide binds to MurF, its terminal carboxylate group is highly likely to coordinate MgII by analogy with the MurD complex. If this is the case, the two reacting groups to form the acyl phosphate intermediate are ligands of MgII in MurF. In this regard, the participation of the carboxylate of UDP-*N*-acetylmuramyl-tripeptide and the γ-phosphate of ATP in MgII coordination has a consequence to locally collect and properly align the two reacting groups. The charge of γ-phosphate is neutralized by multiple interactions with two divalent cations, Lys125, and Asn150, which facilitate the phosphoryl transfer reaction by reducing the charge repulsion between the two negatively-charged reacting groups (the terminal carboxylate of the substrate and γ-phosphate of ATP) in MurF.

The four Mur ligases also share the three-domain modular architecture in which the central and the C-terminal domains have virtually identical topologies. However, they are divided into two groups on the basis of the structural difference in their N-terminal domains with MurC/MurD in one group and MurE/MurF in the other group. In structural aspects, therefore, MurE is most similar to MurF among the four Mur ligases. The crystal structure of the *Ab*MurF–ATP–UDP complex reveals the partial binding mode of UDP-*N*-acetylmuramyl-tripeptide, the substrate of MurF. Interestingly, the binding mode of UDP in the *Ab*MurF–ATP–UDP complex is different from that of UDP in the MurE-UMT (UDP-*N*-acetylmuramyl-L-alanyl-D-glutamate:*meso*-diaminopimelate) complex [25]. In the case of MurE, the uracil ring stacks between Arg29 and Tyr50 that correspond to Arg45 and Phe66, respectively, in MurF. Consequently, UDP interacts only with residues of the N-terminal domain in MurE. In contrast, UDP binds to the border between the N-terminal and the C-terminal domain in MurF. Phe61 and Arg97 interacting with the uracil group and the phosphate moieties of UDP, which are replaced by Ala45 and Asn90 in MurE, are conserved or homologously replaced in the MurF orthologues (Fig. S1), suggesting that the UDP binding mode presented here can be applied to other MurF proteins. The different UDP binding mode indicates that the substrate-binding mode of MurF is different from that of MurE, which may reflect the different length of UDP-precursor substrates of MurE and MurF.

Acknowledgments

This study was supported by the National Research Foundation of Korea Grant NRF-2012R1A2A2A02005978 and the KIOST in-house programs (PE99212 and PE99263).

Appendix A. Supplementary data

Supplementary data associated with this article can be found, in the online version, at http://dx.doi.org/10.1016/j.bbrc.2014.06.108.

References

[1] J.M. Cisneros, M.J. Reyes, J. Pachon, B. Becerril, F.J. Caballero, J.L. GarciaGarmendia, C. Ortiz, A.R. Cobacho, Bacteremia due to *Acinetobacter baumannii* epidemiology, clinical findings, and prognostic features, Clin. Infect. Dis. 22 (1996) 1026–1032.
[2] A.Y. Peleg, H. Seifert, D.L. Paterson, *Acinetobacter baumannii*: emergence of a successful pathogen, Clin. Microbiol. Rev. 21 (2008) 538–582.
[3] H. Seifert, A. Strate, G. Pulverer, Noscomial bacteremia due to Acinetobacter-baumannii. Clinical-features, epidemiology, and predictors of mortality, Medicine 74 (1995) 340–349.
[4] F.S. Taccone, H. Rodriguez-Villalobos, D. De Backer, V. De Moor, J. Deviere, J.L. Vincent, F. Jacobs, Successful treatment of septic shock due to pan-resistant *Acinetobacter baumannii* using combined antimicrobial therapy including tigecycline, Eur. J. Clin. Microbiol. Infect. Dis. 25 (2006) 257–260.
[5] R. Valencia, L.A. Arroyo, M. Conde, J.M. Aldana, M.-J. Torres, F. Fernandez-Cuenca, J. Garnacho-Montero, J.M. Cisneros, C. Ortiz, J. Pachon, J. Aznar, Nosocomial outbreak of infection with pan-drug-resistant *Acinetobacter baumannii* in a tertiary care university hospital, Infect. Control Hosp. Epidemiol. 30 (2009) 257–263.
[6] T.D. Bugg, C.T. Walsh, Intracellular steps of bacterial-cell wall peptidoglycan biosynthesis-enzymology, antibiotics, and antibiotic-resistance, Nat. Prod. Rep. 9 (1992) 199–215.
[7] H. Barreteau, A. Kovac, A. Boniface, M. Sova, S. Gobec, D. Blanot, Cytoplasmic steps of peptidoglycan biosynthesis, FEMS Microbiol. Rev. 32 (2008) 168–207.
[8] K.L. Longenecker, G.F. Stamper, P.J. Hajduk, E.H. Fry, C.G. Jakob, J.E. Harlan, R. Edalji, D.M. Bartley, K.A. Walter, L.R. Solomon, T.F. Holzman, Y.G. Gu, C.G. Lerner, B.A. Beutel, V.S. Stoll, Structure of MurF from *Streptococcus pneumoniae* co-crystallized with a small molecule inhibitor exhibits interdomain closure, Protein Sci. 14 (2005) 3039–3047.
[9] M. Hrast, S. Turk, I. Sosic, D. Knez, C.P. Randall, H. Barreteau, C. Contreras-Martel, A. Dessen, A.J. O'Neill, D. Mengin-Lecreulx, D. Blanot, S. Gobec, Structure-activity relationships of new cyanothiophene inhibitors of the essential peptidoglycan biosynthesis enzyme MurF, Eur. J. Med. Chem. 66 (2013) 32–45.
[10] Y. Yan, S. Munshi, B. Leiting, M.S. Anderson, J. Chrzas, Z. Chen, Crystal structure of *Escherichia coli* UDPMurNAc-tripeptide D-alanyl-D-alanine-adding enzyme (MurF) at 2.3 angstrom resolution, J. Mol. Biol. 304 (2000) 435–445.
[11] S. Favini-Stabile, C. Contreras-Martel, N. Thielens, A. Dessen, MreB and MurG as scaffolds for the cytoplasmic steps of peptidoglycan biosynthesis, Environ. Microbiol. 15 (2013) 3218–3228.
[12] Y.J. An, C.-S. Jeong, J.H. Yu, K.M. Chung, S.-S. Cha, Purification, crystallization and preliminary X-ray crystallographic analysis of the UDP-N-acetylmuramoyl-tripeptide-D-alanyl-D-alanine ligase (MurF) from *Acinetobacter baumannii*, Acta Crystallogr. F Struct. Biol. Cryst. Commun. 70 (2014) 976–978.
[13] T.C. Terwilliger, P.D. Adams, R.J. Read, A.J. McCoy, N.W. Moriarty, R.W. Grosse-Kunstleve, P.V. Afonine, P.H. Zwart, L.-W. Hung, Decision-making in structure solution using Bayesian estimates of map quality: the PHENIX AutoSol wizard, Acta Crystallogr. D Biol. Crystallogr. 65 (2009) 582–601.
[14] P.D. Adams, P.V. Afonine, G. Bunkoczi, V.B. Chen, I.W. Davis, N. Echols, J.J. Headd, L.-W. Hung, G.J. Kapral, R.W. Grosse-Kunstleve, A.J. McCoy, N.W. Moriarty, R. Oeffner, R.J. Read, D.C. Richardson, J.S. Richardson, T.C. Terwilliger, P.H. Zwart, PHENIX: a comprehensive Python-based system for macromolecular structure solution, Acta Crystallogr. D Biol. Crystallogr. 66 (2010) 213–221.
[15] Z. Otwinowski, W. Minor, Processing of X-ray diffraction data collected in oscillation mode, Macromol. Crystallogr. A 276 (1997) 307–326.
[16] A. Vagin, A. Teplyakov, Molecular replacement with MOLREP, Acta Crystallogr. D Biol. Crystallogr. 66 (2010) 22–25.
[17] P. Emsley, K. Cowtan, Coot: model-building tools for molecular graphics, Acta Crystallogr. D Biol. Crystallogr. 60 (2004) 2126–2132.
[18] A.T. Brunger, P.D. Adams, G.M. Clore, W.L. DeLano, P. Gros, R.W. Grosse-Kunstleve, J.S. Jiang, J. Kuszewski, M. Nilges, N.S. Pannu, R.J. Read, L.M. Rice, T. Simonson, G.L. Warren, Crystallography & NMR system: a new software suite for macromolecular structure determination, Acta Crystallogr. D Biol. Crystallogr. 54 (1998) 905–921.
[19] I. Nobeli, R.A. Laskowski, W.S. Valdar, J.M. Thornton, On the molecular discrimination between adenine and guanine by proteins, Nucleic Acids Res. 29 (2001) 4294–4309.
[20] J.A. Bertrand, G. Auger, L. Martin, E. Fanchon, D. Blanot, D. La Beller, J. van Heijenoort, O. Dideberg, Determination of the MurD mechanism through crystallographic analysis of enzyme complexes, J. Mol. Biol. 289 (1999) 579–590.
[21] M.S. Anderson, S.S. Eveland, H.R. Onishi, D.L. Pompliano, Kinetic mechanism of the *Escherichia coli* UDPMurNAc-tripeptide D-alanyl-D-alanine-adding enzyme: use of a glutathione S-transferase fusion, Biochemistry 35 (1996) 16264–16269.
[22] P.J. Falk, K.M. Ervin, K.S. Volk, H.T. Ho, Biochemical evidence for the formation of a covalent acyl-phosphate linkage between UDP-N-acetylmuramate and ATP in the *Escherichia coli* UDP-N-acetylmuramate: L-alanine lipase-catalyzed reaction, Biochemistry 35 (1996) 1417–1422.
[23] S. Vaganay, M.E. Tanner, J. van Heijenoort, D. Blanot, Study of the reaction mechanism of the D-glutamic acid-adding enzyme from *Escherichia coli*, Microb. Drug Resist. 2 (1996) 51–54.
[24] S. Dementin, A. Bouhss, G. Auger, C. Parquet, D. Mengin-Lecreulx, O. Dideberg, J. van Heijenoort, D. Blanot, Evidence of a functional requirement for a carbamoylated lysine residue in MurD, MurE and MurF synthetases as established by chemical rescue experiments, Eur. J. Biochem. 268 (2001) 5800–5807.
[25] E. Gordon, B. Flouret, L. Chantalat, J. van Heijenoort, D. Mengin-Lecreulx, O. Dideberg, Crystal structure of UDP-N-acetylmuramoyl-L-alanyl-D-glutamate: *meso*-diaminopimelate ligase from *Escherichia coli*, J. Biol. Chem. 276 (2001) 10999–11006.